Characterization and molecular basis of the oligomeric structure of HIV-1 Nef protein

Stefan Arold, François Hoh, Stephanie Domergue, Catherine Birck, Marc-André Delsuc, Magali Jullien, Christian Dumas

▶ **To cite this version:**

HAL Id: hal-02359568

https://hal.archives-ouvertes.fr/hal-02359568

Submitted on 13 Nov 2019

Characterization and molecular basis of the oligomeric structure of HIV-1 Nef protein

STEFAN AROLD,[1,3] FRANÇOIS HOH,[1] STEPHANIE DOMERGUE,[1] CATHERINE BIRCK,[2]
MARC-ANDRÉ DELSUC,[1] MAGALI JULLIEN,[1] AND CHRISTIAN DUMAS[1]

[1]Centre de Biochimie Structurale, UMR C5048 CNRS, U414 INSERM, Université Montpellier I,
 Avenue C. Flahault, 34060 Montpellier, France
[2]Groupe de Cristallographie Biologique, IPBS-CNRS, 31077 Toulouse, France

Abstract

The Nef protein of human immunodeficiency virus type I (HIV-1) is an important determinant for the onset of AIDS disease. The self-association properties of HIV-1 Nef are analyzed by chemical cross-linking, dynamic light scattering, equilibrium analytical ultracentrifugation, and NMR spectroscopy. The experimental data show that the HIV-1 Nef core domain forms stable homo-dimers and trimers in solution, but not higher oligomers. These Nef homomers are not covalently linked by disulfide bridges, and the equilibrium between these forms is dependent on the Nef concentration. We further provide the molecular basis for the Nef core dimers and trimers obtained by analysis of crystallographic models. Oligomerization of biological polypeptides is a common tool used to trigger events in cellular signaling and endocytosis, both of which are targeted by Nef. The quaternary structure of Nef may be of physiological importance and may help to connect its cellular targets or to increase affinity of the viral molecule for its ligands. The herein described models for Nef dimers and trimers will allow further mutational studies to elucidate their role in vivo. These results provide novel insight into the structural and functional relationships of this important viral protein. Moreover, the oligomer interface may represent a novel target for the design of antiviral agents.

Keywords: chemical cross-linking; dynamic light scattering; HIV-1; Nef; NMR; oligomerization; sedimentation equilibrium

The *nef* gene of human and simian immunodeficiency virus (HIV and SIV, respectively) is an essential determinant for the onset of the acquired immunodeficiency syndrome (AIDS) in vivo (Deacon et al., 1995; Kirchhoff et al., 1995; Mariani et al., 1996; Hanna et al., 1998).

The *nef* gene encodes a 27 kDa auxiliary protein that is expressed at high levels early in the viral replication cycle. The Nef protein has a number of distinct activities that contribute to its potential to increase viral replication and pathogenicity. Nef downregulates cell surface CD4 and MHC-I molecules by accelerating the rate of their endocytosis from the cellular membrane (Aiken et al., 1994; Garcia & Miller, 1994; Schwartz et al., 1996; Craig

et al., 1998). Nef enhances virion infectivity (Chowers et al., 1994; Miller et al., 1994; Schwartz et al., 1995) and alters cellular signal transduction and activation, possibly mediated by interactions with cellular kinases via the SH3-binding P-x-x-P motif of Nef (Baur et al., 1994; Du et al., 1995; Greenway et al., 1995; Lee et al., 1995; Saksela et al., 1995; Collette et al., 1996). Nef has no enzymatic activity; its action is therefore based on association with host cell proteins or viral components. Many putative cellular Nef targets have been reported so far, including proteins of signal transduction pathways such as tyrosine and serine kinases (Saksela, 1997), and components of the endocytotic machinery, such as subunits of adaptor protein complexes (Le Gall et al., 1998; Piguet et al., 1998), a thioesterase (Liu et al., 1997), and β-cop (Benichou et al., 1994; Piguet et al., 1999). Nef appears also to display a weak affinity for the cytoplasmic tail of CD4 (Harris & Neil, 1994; Grzesiek et al., 1996b; Rossi et al., 1996).

HIV and SIV Nef proteins consist of a conserved core domain of about 120 residues and two highly divergent and disordered regions, i.e., the N-terminus (the first 68 to 100 amino acids, depending on the viral family) and a 30 amino acid loop projecting from the core domain. The N-terminus of all Nef proteins is myristoylated and mediates membrane association. The core domain

of Nef folds into a globular α-β protein, whereas the N-terminal and central loop region, i.e., 50% of the polypeptide chain, seem to be unstructured in an aqueous solvent (Grzesiek et al., 1996a; Lee et al., 1996; Arold et al., 1997; Barnham et al., 1997; Geyer et al., 1999).

Nef proteins are found incorporated in the HIV-1 viral particles and are cleaved by the viral protease (Freund et al., 1994a, 1994b; Gaedigk-Nitschko et al., 1995; Pandori et al., 1996; Schorr et al., 1996; Welker et al., 1996; Miller et al., 1997; Chen et al., 1998). Incorporation and proteolytic cleavage in virions have equally been reported for HIV-2 Nef (Schorr et al., 1996). The functional significance of the cleavage, which liberates the C-terminal core domain from its membrane associated N-terminus, remains unknown. Intriguingly, SIV Nef proteins lack this cleavage site.

Oligomerization of HIV-1 Nef expressed in bacteria and eucaryotic cells has first been reported by Kienzle et al. (1993). Homomeric Nef dimers, trimers, and higher oligomers were subsequently reported on the surface of infected HeLa CD4+ cells (Fujii et al., 1996). Both groups observed Nef oligomers under reducing and nonreducing conditions, indicating that these oligomers can form without stabilization by disulfide bonds. Additionally, Nef core domain dimerization was reported using NMR spectroscopy (Grzesiek et al., 1997) and the structures of two crystal forms of HIV-1$_{lai}$ Nef (Arold et al., 1997) reveal dimeric and trimeric packing.

Determination of the oligomeric states of Nef is important for understanding more precisely the molecular mechanism of Nef functions. To address this issue, we combined biochemical and biophysical experiments with analysis of structural data obtained by crystallography. We found that the conserved core domain of HIV-1 Nef corresponding to the product of proteolytic cleavage of Nef by the viral protease, suffice to form stable dimers and trimers in vitro. The homomer interface is formed in both oligomeric states by basically the same amino acids, which are well conserved in HIV-1 isolates. These residues could represent "hot spots" to be probed by mutagenesis and, if oligomerization proves to be important for the action of HIV-1 Nef, they may represent novel targets for drug intervention.

Results

Data were collected on three different HIV-1$_{lai}$ Nef constructs: Nef full length, Nef$_{\Delta 1,57}$, i.e., the core domain corresponding to the product of proteolytic cleavage by HIV-1 protease, and Nef$_{\Delta 1-56, \Delta 206}$. In Nef$_{\Delta 1-56, \Delta 206}$ the only solvent accessible cysteine (C206) of the core domain has been deleted to preclude oligomerization by disulfide bond formation. Additionally, the N-terminus has been extended by a tryptophane residue (W57) immediately upstream of the cleavage site. According to NMR studies, W57 may be required to anchor the flexible segment between the protease cleavage site (W57, L58) and the P-x-x-P motif region (residues 71–77) to the folded core of Nef (Grzesiek et al., 1996a, 1997). In accordance with other authors (Lee et al., 1996), we refer herein to both Nef$_{\Delta 1-57}$ and Nef$_{\Delta 1-56, \Delta 206}$ as "Nef core domain."

The HIV-1 Nef core domain alone forms dimers and trimers

To address the question of whether the core domain of Nef is sufficient to promote oligomer formation, we carried out cross-linking studies with glutaraldehyde as described in Materials and methods. To exclude oligomerization due to nonspecific disulfide bond formation, we based our analysis on the Nef$_{\Delta 1-56, \Delta 206}$ mutant.
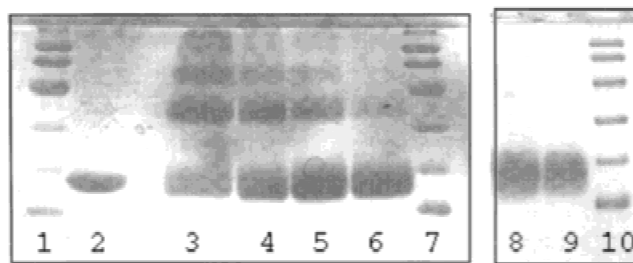
SDS-PAGE analysis of the cross-linked Nef core domains (Fig. 1) revealed monomeric (18 kDa), dimeric (37 kDa), and trimeric (56 kDa) protein, supporting that the flexible N-terminus is not required for oligomer formation. Figure 1 shows that the protein is predominantly monomeric in Lane 6, dimeric and trimeric in Lane 3. Moreover, the cross-linking experiments indicated that the ratio monomer:dimer:trimer is dependent on protein concentration. This assay will not give a quantitative estimation of the actual quaternary structure of Nef in the range of concentration used. The cross-link experiment will trap the oligomers that are normally in a dynamic equilibrium with the monomers. To rule out the possibility that the observed oligomerization was an artifact due to Nef purification and storage, we performed chemical cross-linking experiments with two Nef preparations (data not shown) and obtained similar patterns. Only monomers were observed in similar experiments (Fig. 1: Lanes 8, 9) with unfolded Nef protein.

The oligomeric state of Nef core is concentration dependent

Dynamic light scattering

We next investigated the concentration dependence of the oligomeric state of Nef core domain. To this end, we first employed Dynamic Light Scattering (DLS). DLS is a rapid and nondestructive method to measure simultaneously and independently the size distribution, the molecular weight, and the translational diffusion coefficient D_τ of a protein in solution without calibration. From D_τ, an apparent hydrodynamic diameter d_H can be calculated using the Stokes–Einstein equation, $d_H = 2k_B T/(6\pi\eta_0 D_\tau)$, where k_B is Boltzmann's constant, T is the temperature in K, and η_0 is the solvent viscosity. The apparent molecular weight correlates with the total amount of light scattered and is independent of the shape of the protein.

As we already reported previously (Franken et al., 1997), the size distribution of full length Nef was broad and irregular, even under strong reducing conditions (5 mM dithiothreitol (DTT)) and at low protein concentration (0.1 mM), revealing a strong propensity to form high molecular weight aggregates. Under the same conditions, the Nef core domains show a single broad peak corresponding to a diameter of 7 and 5.2 nm for Nef$_{\Delta 1,57}$ and

Fig. 1. Analysis of cross-linking by glutaraldehyde. The Nef core domain correspond to Nef$_{\Delta 1-56, \Delta 206}$. The SDS-PAGE gels (Lanes 1, 7, 10) contains molecular mass markers (14, 21, 30, 46, 66, and 97 kDa), Nef core domain (Lane 2), Nef core domain reacted with glutaraldehyde (Lanes 3–6) with respective Nef concentrations of 100, 20, 10, and 2.5 μg/mL and glutaraldehyde concentration of 2%. As negative control, the Nef core domain was heated at 60 °C for 20 min (Lane 8) or diluted at low ionic strength (Lane 9) prior to cross-linking by glutaraldehyde. All the reactions are in phosphate buffer 50 mM (5 mM for Lane 9), pH 8.0, incubation time 12 h at room temperature.

Nef$_{\Delta1-56,\Delta206}$, respectively (data not shown). The difference in the apparent hydrodynamic diameter of the two constructs may be explained by the fact that in absence of W57, the flexible segment between L58 and the P-x-x-P motif is not anchored to the core domain, leading to a greater hydrodynamic radius and larger solvent exposed surface area for Nef$_{\Delta1,57}$.

The exclusion of disulfide bond formation led us to use the Nef$_{\Delta1-56,\Delta206}$ construct to investigate the concentration dependence of the quaternary structure of the Nef core domain. The apparent diameter and the molecular weight of Nef$_{\Delta1-56,\Delta206}$ were measured for protein concentrations from 55 μM to 1 mM. Within this concentration range, the diameter and the molecular weight increase with concentration (Fig. 2). Both the molecular weight and the diameter transitions are smooth and slow, suggesting that, at least, two species coexist in a concentration-dependent equilibrium within the used concentration range. Consequently, the measured
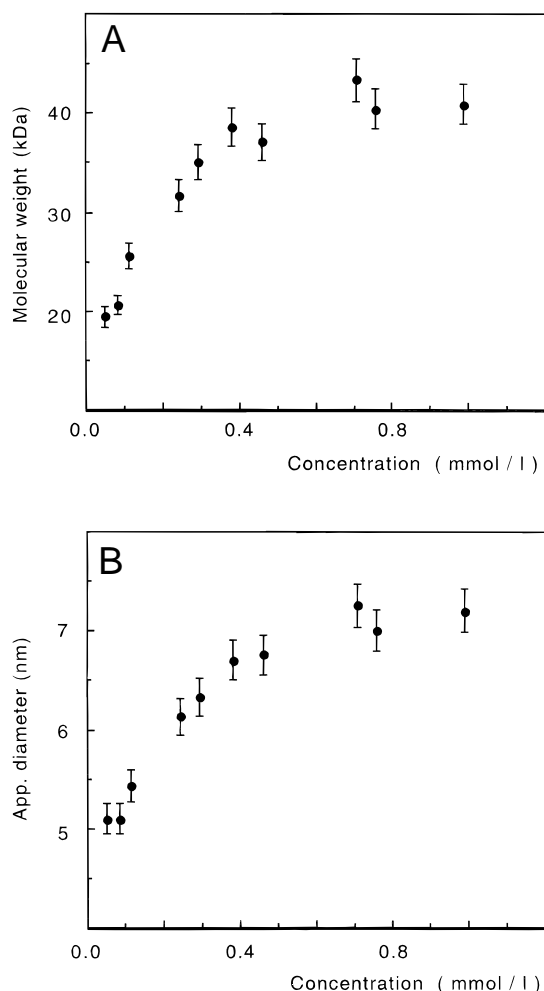
Fig. 2. Concentration dependence of (**A**) the apparent molecular weight and (**B**) hydrodynamic diameter of Nef$_{\Delta1-56,\Delta206}$ assessed by dynamic light scattering at 20 °C. The apparent weight and diameter represent the weighted mean of the solute species. Due to the 30 amino acid solvent exposed loop, Nef$_{\Delta1-56,\Delta206}$ is not an ideal globular protein. The apparent hydrodynamic diameter is therefore larger than calculated for a globular protein of the size of Nef core (see text). Both diameter and molecular mass indicate a transition between a monomeric and an oligomeric state of Nef$_{\Delta1-56,\Delta206}$. The solvent is 10 mM Tris-HCl, pH 8, 150 mM NaCl, and 2 mM EGTA.

values represent the weighted mean of the different solute species. Coexistence of several oligomeric states may thus lead to an over- and underestimation of the DLS parameters of the low- and high-concentration species, respectively.

We next tried to establish what oligomeric states underlie the obtained DLS data. The observed molecular weight tends toward 19 kDa below a concentration of 100 μM, whereas above 700 μM the molecular weight reaches 40 kDa (Fig. 2). Given the molecular mass calculated from the amino acid composition (17.7 kDa) for Nef$_{\Delta1-56,\Delta206}$, DLS data indicate that this core domain is predominantly in the monomeric state below 100 μM with possibly a very small population of oligomeric Nef. Above a protein concentration of 700 μM, the determined apparent molecular weight is more than twice the monomeric mass, suggesting a mixture of dimeric ($M_r = 35.2$ kDa) and trimeric ($M_r = 52.8$ kDa) Nef core domains (Fig. 2A).

We next analyzed the independently measured hydrodynamic diameter. The changes in diameter correlate with the molecular weight changes. At concentrations below 100 μM, the mean diameter tends toward a limit of 5 nm, whereas at concentrations above 700 μM, the apparent diameter stabilizes around 7.2 nm (Fig. 2B). Assuming a spherical shape and a typical hydration level of 0.3 g of water per g of protein, we calculated the hydrodynamic diameters of 4, 5.6, and 6.5 nm for the Nef core monomer, dimer, and trimer, respectively (for calculation of the hydrodynamic diameter of oligomers, see Garcia Bernal & Garcia de la Torre, 1981). Due to the central 30 amino-acid loop (residues 149–178), the shape of Nef is not spherical and hydrodynamic diameters are higher than calculated for a globular protein. However, the mean values measured for low and high protein concentration approach the diameters of the monomer and the trimer, respectively. From the data, though, it seems that dimers persist at the lowest used concentration. Further analysis of the size distribution of Nef$_{\Delta1-56,\Delta206}$ at 1 mM revealed that at least two populations still coexist at the high concentration end of our data: a predominant species with a diameter of ~9 nm, and a second centered around 5 nm (data not shown). This size distribution analysis is not precise for small molecules and provides rather qualitative evidence for the coexistence of at least two species (the larger peak at 9 nm probably already harbors two species, i.e., dimers and trimers), rather than their exact diameter.

In summary, DLS data indicate a monomeric Nef core below 0.1 mM. At higher concentrations dimers and trimers are formed, the equilibrium between these forms being dependent on the Nef concentration. This behavior is consistent with chemical cross-linking experiments.

Analytical ultracentrifugation

Sedimentation equilibrium is also a powerful technique to analyze associating systems and define equilibrium constants involved in a self-association process (Hensley, 1996). Eight datasets at six concentrations and two rotor speed (see Materials and methods) were analyzed simultaneously using the discrete self-association models with defined stoichiometry (Johnson et al., 1981). Assuming a unique species with ideal behavior provided a poor fit (non-random distribution of the residuals with typical pattern indicating association) and a molecular mass of ~22,500 Da. This value is inconsistent with both a monomer and a dimer. A good fit (RMS = 0.012) was obtained employing a monomer–dimer self-association model ($k_2 = 2.02 \times 10^3$ M^{-1}). However, a slightly better fitting in terms of both lower variance (RMS = 0.010) and random distri-

bution of residuals were obtained with a multiple equilibria model (monomers, dimers, and trimers) than with the single monomer to dimer equilibrium. This fit yielded an association constant $k_2 = 1.65 \times 10^3 \ M^{-1}$ for monomer–dimer equilibrium and $k_3 = 5.67 \times 10^6 \ M^{-2}$ for monomer–trimer equilibrium. Attempts to fit the data including tetrameric species failed. Figure 3 shows the sedimentation equilibrium data for Nef core domain. Molecular mass was fixed to that of the monomer, calculated from the amino acid composition (17,700 Da). The value of second virial coefficient obtained by the fitting algorithm ($B = 1.5 \times 10^{-8}$) indicates that nonideality is not significant during Nef association. In the range of concentration used, monomers, dimers, and trimers of Nef core domain coexist in equilibrium with each other.

NMR DOSY

To investigate the oligomeric state in solution, we also measured the diffusion coefficient D_τ of Nef using NMR experiments of the DOSY type. The Stokes–Einstein equation for free diffusion of solute molecules in a solvent relates the observed diffusion coefficient to the friction force of the solvent on the molecule due to the viscous drag of the solvent on the molecular surface. This friction force can be derived from the geometry of the diffusing molecules in the case of simple shapes (Johnson & Gabriel, 1981). In the general case, it was proposed to relate the observed diffusion on the solvent accessible surface area (SASA) (Krishnan & Cos-

man, 1998). This approach is extended here to the case of translational diffusion. Changes in D_τ can therefore monitor changes in the oligomeric state of a molecule in solution. Using an empirical relation between D_τ and SASA previously established by measuring the diffusion coefficient of 15 proteins with known structures and oligomeric states (M.-A. Delsuc, unpubl. data), we measured the diffusion coefficients and calculated the SASAs for solubilized Nef constructs. Similarly, we have calculated apparent molecular weights M_{app}. However, and in contrast to SASAs, the relation between D_τ and M_{app} is based on the assumption that the solute molecules are rigid and globular. Due to the large solvent exposed central loop region (residues 149–178), neither approximation is fully satisfied by Nef.

We measured the diffusion coefficient of Nef$_{\Delta1-56,\Delta206}$ at concentrations of 140 and 560 μM, despite the lower concentration limit being the sensitivity of the technique on our equipment. We first measured the overall diffusion coefficient D_τ observed in the complete spectra, thus taking into account only the predominant solute population and ignoring minor ones (Fig. 4; Table 1). The diffusion coefficient changed from $80.4 \pm 1.6 \ \mu m^2/s$ to $69.2 \pm 1.8 \ \mu m^2/s$ on going from low to high concentration (Table 1), indicating a significantly larger SASA at higher concentration.

Detailed analysis of NMR data recorded at 140 μM Nef reveals three populations with distinct diffusion coefficients (P1, S, and P2 in Table 1). At a concentration of 560 μM, the population with
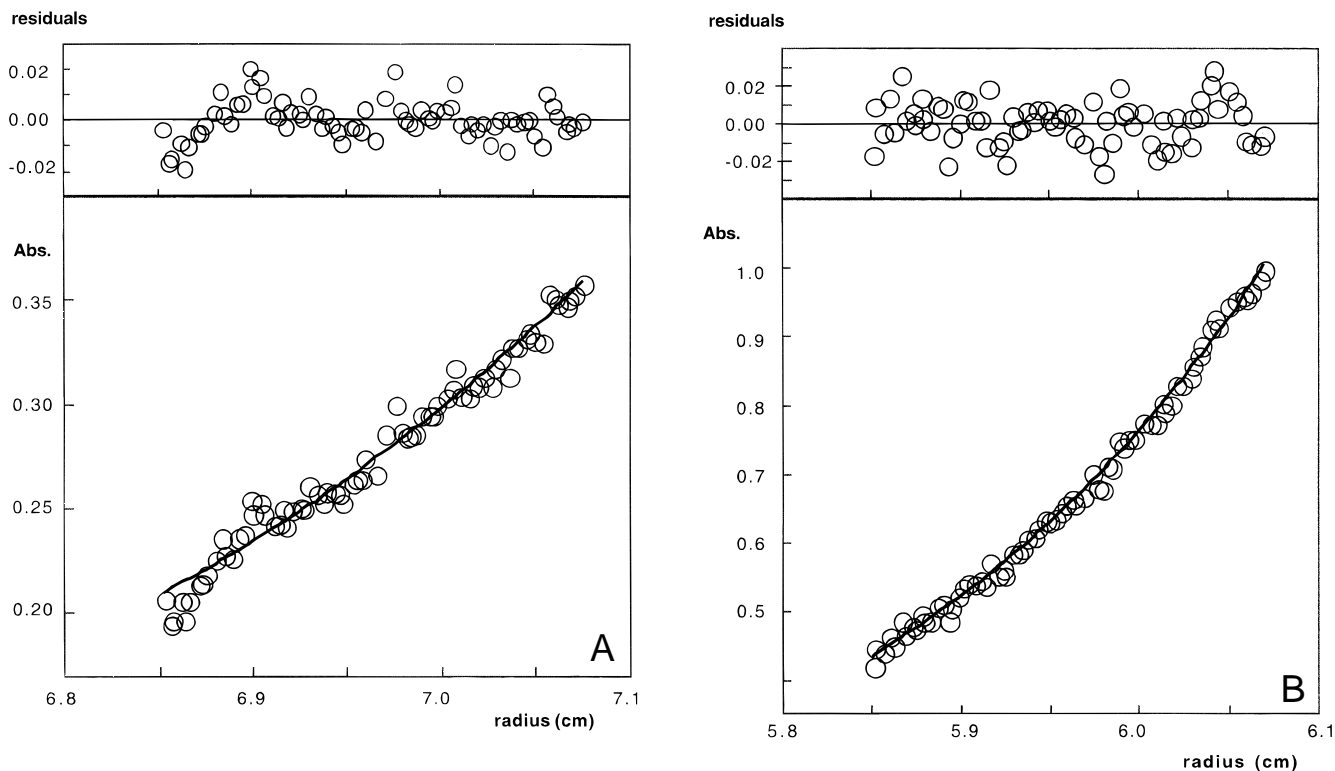
Fig. 3. Sedimentation equilibrium data of Nef core domain plotted as concentration (in A_{302} units) vs. radial position profile (r in cm). Samples of HIV-1$_{Lai}$ Nef$_{\Delta1-56,\Delta206}$ in 20 mM Tris-HCl, pH 7.5, NaCl 100 mM were subjected to centrifugation at 15,000 and 12,000 rpm as described in Materials and methods. Loading concentration of Nef are in (**A**) 0.23 mM at 12,000 rpm and (**B**) 0.45 mM at 15,000 rpm. For each sample, the resulting data and the corresponding fitted curve are shown in the lower panel. The solid line was simulated by using the parameters obtained from global analysis of eight datasets (six loading concentrations at 15,000 rpm and two at 12,000 rpm) with a three-species model (monomer, dimer, and trimer). The corresponding top panels in **A** and **B** illustrate the residuals of the fits of these two datasets as a function of radial position.
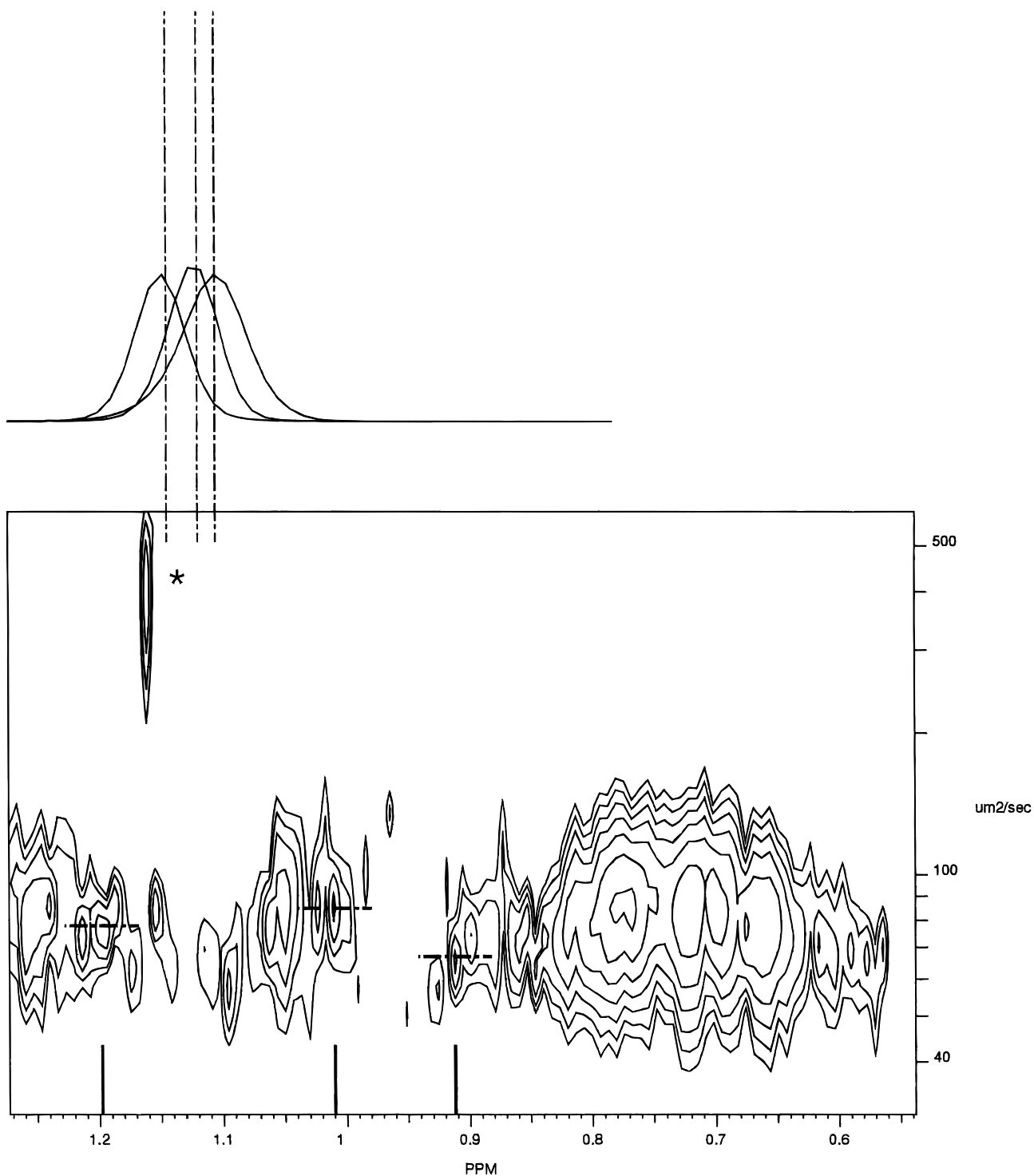
Fig. 4. Analysis of the oligomeric state based on NMR DOSY data: the methyl region of the DOSY spectrum of Nef$_{\Delta 1-56,\Delta 206}$ at 140 μM is shown. Three columns have been extracted at 0.91, 1.01, and 1.20 ppm and are reported to the left. The corresponding diffusion coefficients, materialized by hatched axes, are 66, 84, and 77 mm^2/s, respectively. The star indicates an impurity, with a much faster diffusion coefficient.

highest diffusion coefficient (P1) is no longer observed, whereas populations with diffusion coefficients corresponding to S and P2 were detected. The SASA calculated from the population with the highest diffusion coefficient (P1; SASA = 8,150 Å^2) is smaller than the SASA calculated for dimeric Nef models (Table 2), we therefore attributed it to a monomeric state of Nef. Consequently, the SASA of the dimer can be calculated as [(2 × SASA monomer) − (calculated buried interface)], i.e., 15,300 Å^2. This SASA

Table 1. *Diffusion coefficients for Nef$_{\Delta1-56,\Delta206}$ based on NMR DOSY data*[a]

	D (μm^2/s)	Apparent SASA (Å^2)	Apparent Mw (kDa)
Nef full length			
S	70 ± 2	11,700	30
Nef$_{\Delta1-56,\Delta206}$ at 140 μM			
P1	84 ± 4	8,150	18
S	77 ± 4	9,680	23
P2	66 ± 4	12,500	33
Nef$_{\Delta1-56,\Delta206}$ at 560 μM			
P1	—	—	—
S	74 ± 2	10,500	26
P2	64 ± 2	14,010	39
Nef$_{\Delta1-56,\Delta206}$ calculated from P1 at 140 μM			
Monomer	84	8,150	18
Dimer	61	15,300	45
Trimer	51	22,000	76

[a]SASAs were derived from the diffusion coefficients as described in Materials and methods. P1, obtained from distinct population with high diffusion coefficient; P2, from distinct population with low diffusion; S, obtained from gross peaks, ignoring distinct peaks (P1 and P2). This value corresponds to the superimposition of the contributing populations and represents their weighted mean. Nef$_{\Delta1-56,\Delta206}$ calculated corresponds to the values obtained for dimers and trimers, assuming that D of population P1 at 140 μM corresponds to the diffusion coefficient of the monomer.

is approximately equivalent to that of P2, indicating that P2 corresponds to dimeric Nef. The buried surface area derived from $[(2 \times P1) - P2]$ is ~1,900 Å^2, which is larger than calculated from crystallographic models (Table 2). However, the errors attached to SASAs are too large to allow further exploitation of this observation. Consistently, molecular weights of small (P1) and large species (P2) correspond to the molecular weights expected for Nef$_{core}$ monomer (17.7 kDa) and dimer (35.4 kDa), respectively. The spe-

Table 2. *Calculated SASAs of Nef models*[a]

Model	Calculated SASA (Å^2)		
	Monomer	Dimer	Trimer
Nef$_{\Delta1-70,\Delta149-177,\Delta203-206}$	6,000	10,980	16,700
Nef$_{\Delta1-56,\Delta159-173}$	10,140	19,260	29,120
Nef$_{\Delta1-56,\Delta206}$	11,900	22,700	34,300
Nef full length	18,200	35,400	53,400

[a]The models represented in are as follows: Nef$_{\Delta1-70,\Delta149-177,\Delta203-206}$, the crystallographic models (dimer corresponds to PDB entries 1efn and 1avz, trimer is derived from 1avv); Nef$_{\Delta1-56,\Delta159-173}$ model derived from the NMR structure (PDB entry 2nef). The central loop region is completely solvent exposed, but truncated; Nef$_{\Delta1-56,\Delta206}$, model derived from the NMR structure (PDB entry 2nef). The central loop has been manually completed, assuming it being completely solvent exposed; Nef full length, derived from the combination of NMR structures 2nef, 1qa4, and 1qa5, the central loop region has been manually completed, assuming it completely solvent exposed.

cies (S) can be assigned to the superimposition of peaks from oligomeric and monomeric Nef on the NMR spectra.

Only hints for trimeric Nef can be found in the spectra (see Fig. 4, lines at 0.93 and 1.10 ppm for instance) but could not be fully analyzed because of a too low signal-to-noise ratio. This is explained by the inherent characteristics of the DOSY spectra: First, DOSY measures an apparent diffusion for each peak of the spectrum. To separate monomers, dimers, and trimers, specific peaks have to be present for each species. As dimer and trimer interfaces are formed by mostly the same residues (see below), it is likely that peaks for dimeric and trimeric Nef partly superimpose. Second, as with most NMR measurements, the sensitivity of DOSY decreases with the size of the molecules. Trimers will give a much weaker signal than dimers.

Interestingly, the SASAs of Nef core monomers and dimers (Table 1) are significantly smaller than the SASA calculated from models (Table 2) assuming a solvent exposed loop region. Likewise the increase in SASA calculated for full length Nef is smaller than expected when assuming a completely solvent exposed N-terminus (the SASA for the N-terminus only is ~6,300 Å^2). Moreover, the molecular weights derived for Nef core monomers and dimers on the basis of the measured diffusion assuming a globular protein do not differ greatly from the molecular weights expected for Nef core monomers and dimers. Taken together, our data suggest that the flexible parts of Nef, which contain important motifs for interaction with cellular partners, e.g., the membrane targeting site on the N-terminus (Geyer et al., 1999) and the dileucine based endocytosis motif (Bresnahan et al., 1998; Craig et al., 1998; Greenberg et al., 1998a), do not float freely in the surrounding solvent, but are partially attached to the core domain.

Molecular basis for Nef core dimers and trimers

We have solved the crystal structure of HIV-1 Nef$_{\Delta1,57}$ in two different space groups, hexagonal (P6$_5$22) and cubic (P23) (Arold et al., 1997). Nef crystals analogous to our hexagonal crystals have previously been reported by Lee et al. (1996). In all Nef crystals, the buried surface between adjacent Nef molecules is large, involving about 8–9% of the total accessible surface area. However, the constellations of adjacent Nef molecules in the different crystal forms are not the same. The packing of the Nef core molecules in the cubic form could be interpreted as Nef forming trimers, related by crystallographic symmetry, whereas the two Nef molecules of the hexagonal asymmetric unit associate as a dimer related by a local twofold axis (Fig. 5). In the light of the herein reported experimental evidence for Nef core dimers and trimers in solution, we engaged in a detailed analysis of the crystal contacts to establish if the "crystal oligomers" correspond to the oligomers observed in vitro.

In both the dimeric and trimeric arrangements, it is the same region of Nef that is involved in homologous contacts, implicating residues located in the αB helix and the coil connecting helix αB with strand βA (Figs. 5, 6). The contacts are principally established by the same amino acids in both space groups: R105, D108, I109, L112, Y115, H116, F121, P122, and D123 (Figs. 5, 6). These residues are conserved among HIV-1 Nef isolates and form a hydrophobic core (with a hydrophobic "hot spot" central to Y115, F121, and P122) surrounded by charged amino acids (R105, D108, and D123). Charge complementarity between Nef protomers is achieved by electrostatic interactions between R105 and D123. The association of the two Nef molecules in the hexagonal crystal
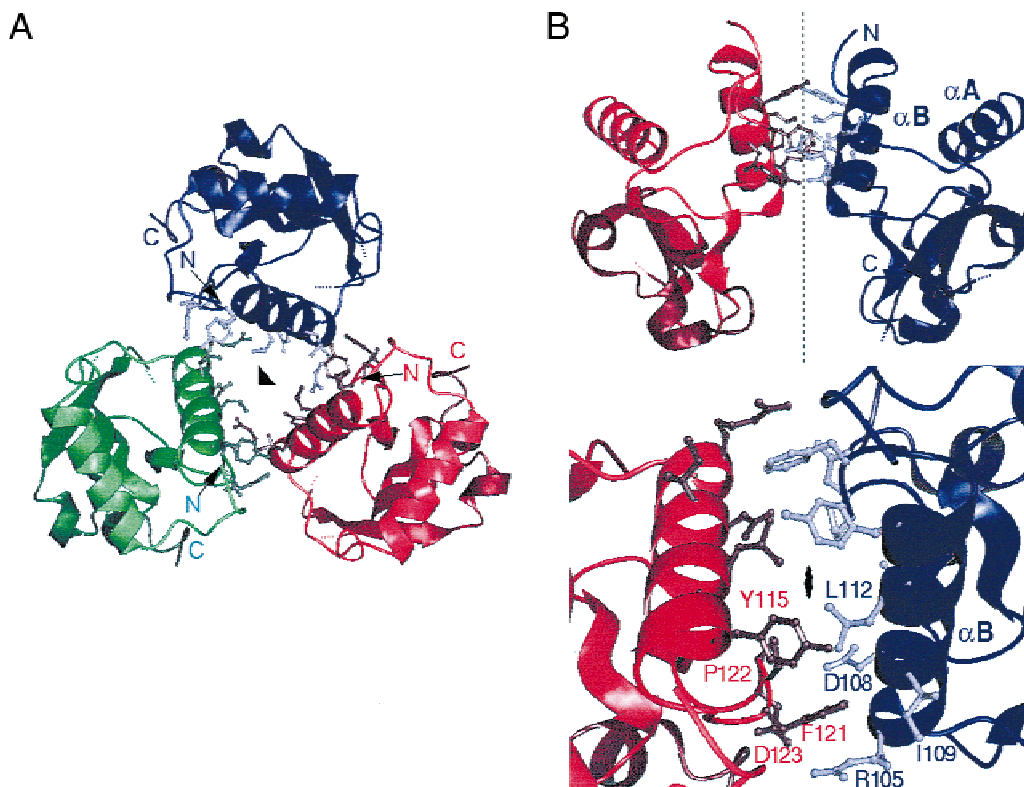
Fig. 5. Molecular basis for Nef core dimers and trimers. **A:** Dimeric Nef core arrangements observed in hexagonal crystals. **B:** Trimeric constellation in cubic Nef core crystals. The figures were prepared with AESOP (M.E. Noble, unpubl. data) and show secondary structure features and the side chains of the amino acids principally involved in homomeric contacts. The (crystallographic) threefold and the (local) twofold axes are indicated for trimeric and dimeric Nef core, respectively.

form buries a surface area of 900 Å^2. In the more densely packed P23 crystal, the trimer interface covers close to 1,300 Å^2 of the solvent accessible surface (430 Å^2 per monomer). The surface buried at the interface is at the lower limit of common protein–protein interfaces (Janin & Chothia, 1990; Jones & Thornton, 1997). This suggests relatively weak interactions, confirmed by the slow dynamic equilibrium between monomeric and oligomeric states within the investigated range of protein concentration.

Evaluation of the models

The following facts made us conclude that the oligomeric arrangements in the crystals correspond to the Nef oligomers observed in solution: (1) The crystals grew out of solutions where Nef is already in part present in its dimeric or trimeric form, with initial Nef concentrations in the crystallization drops of 150 μM for the hexagonal space group and 300 μM for the cubic space group; (2) the residues implicated in oligomerization are conserved in HIV-1 Nef isolates; and (3) the interface buried in the crystalline Nef dimers and trimers suffice the criteria established for homomeric assemblies (Chothia & Janin, 1975; Carugo & Argos, 1997; Jones & Thornton, 1997; Conte et al., 1999). These criteria are as follows: (1) The accessible surface buried upon oligomerization falls within the limits of total buried surface area and of percent of buried surface to total accessible surface observed for homomeric proteins (Jones & Thornton, 1997). (2) The amino acid composition and the shape of the interface are conform to those most

frequently observed in protein–protein assemblies, i.e., phenylalanine, leucine, and isoleucine forming a flat hydrophobic core that is flanked by charged amino acids (arginine, aspartic acid) (Chothia & Janin, 1975; Jones & Thornton, 1997). (3) The secondary structural motifs involved in the homomer interface are helix and coil, which are those who are most frequently observed in homodimeric interfaces (Jones & Thornton, 1997). (4) The molecules are related by a proper symmetry axis, i.e., a rotation axis without translation (Janin & Rodier, 1995).

For completeness, we note that in the cubic crystals, crystallographic symmetry-related molecules pack also as dimers that bury a total of 910 Å^2 of solvent accessible surface area of the protomers. Major contributions to the buried surface area are made by the residues F139, R188, F191, H192, H193, R196, and E197. However, of these, only F139 and H192 are conserved in HIV-1 Nef alleles. Consequently, we classified this dimeric arrangement as a biologically irrelevant result of crystal packing.

Oligomeric state of HIV-1 Nef and functional data

To establish if the homomeric arrangements of Nef described here exclude binding to its putative partners, we visualized the oligomers and investigated the accessibility of the amino acids that are involved in heterologous interactions.

Both oligomeric states leave the SH3 binding site (including the P-x-x-P motif), the protease cleavage site (residues W57 and L58), the acidic cluster between the P-x-x-P motif and the protease cleav-
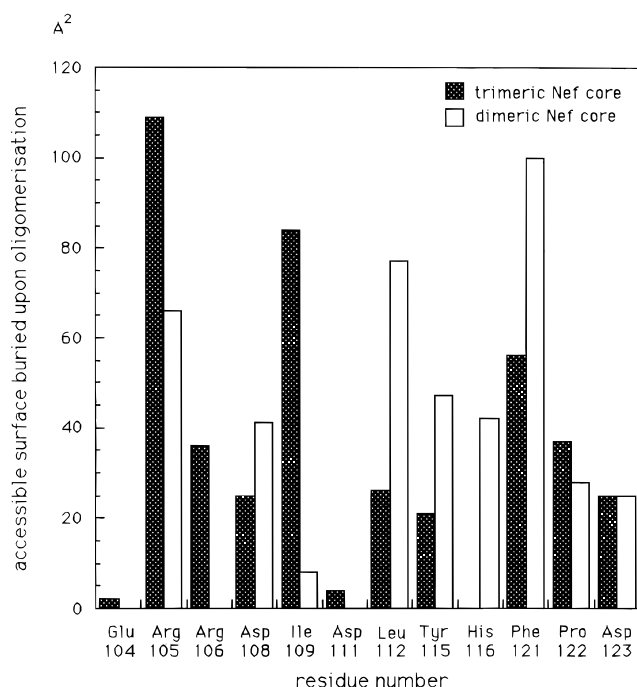
Fig. 6. Solvent accessible surface areas (SASAs) buried per residue upon formation of dimeric Nef core (empty boxes) and trimeric Nef core (dark boxes). The accessible surface areas were calculated using a rolling sphere with a radius of 1.4 Å.

age site, the hydrophobic grove located between the α-helices αA and αB, the central loop region (residues 149–178) and the C-terminus accessible to solvent. Consequently, the configuration of the dimeric and trimeric states of the Nef core domain does not interfere a priori with the recruitment of the SH3 domains (Lee et al., 1996; Arold et al., 1997), CD4 (Grzesiek et al., 1996b), MHC-I (Greenberg et al., 1998b), and adaptin complexes (Greenberg et al., 1997, 1998a; Bresnahan et al., 1998; Craig et al., 1998). It has to be noted that in the di-arginine motif (residues 105–106), which is required for CD4 down-regulation (Wiskerchen & Cheng-Mayer, 1996; Iafrate et al., 1997), is partially implicated in the interface between monomers. Additionally, the trimeric arrangement allows only unstructured or α-helical peptide ligands to access the zone for the putative direct interaction with CD4 (Grzesiek et al., 1996b), but not to larger tertiary structures. Structural analysis of a peptide-mimic of the cytoplasmic tail of CD4 however indicated that it adopts either a random coil conformation in aqueous solution (J.L. Pons & M.-A. Delsuc, unpubl. data) or partially a α-helix conformation in 2,2,2 trifluoroethanol (Wray et al., 1998).

Discussion

The ability of Nef to adopt multimeric structures was assessed by both chemical cross-linking, dynamic light scattering, ultracentrifugation at sedimentation equilibrium, and NMR DOSY experiments. We have demonstrated that, in solution, Nef exist in several discrete oligomeric species, namely monomers, dimers, and trimers. Thus, HIV-1 Nef core domain suffices to form noncovalently linked dimers and trimers that are in a concentration dependent equilibrium with monomers. According to a monomer-dimer-n-

mer self-association model, the association constants are in the order of 1,653 M^{-1} for k_2 and 5.67×10^6 M^{-2} for k_3. Nef core is essentially in a monomeric state only below a concentration of 100 μM. At higher concentrations, in the concentration range of 400 to 800 μM, the solution behaves as an equal mixture of monomeric, dimeric, and trimeric species. A strong indication of the reversibility of the auto-association reaction is related to the fact that multiple sets of sedimentation data, obtained at different loading concentrations, as well as two rotor speeds, could be simultaneously fitted to a single set of equilibrium constants. We further provided a molecular basis for homomer formation of the Nef core domain obtained by analysis of crystal structures.

Our observations are compatible with NMR data on HIV-1 Nef$_{\Delta2–39,\Delta159–173}$ reported by Grzesiek et al. (1997). They determined by NMR relaxation experiments that their Nef construct is monomeric only below 0.1 mM. However, different from the herein reported dimeric and trimeric states of Nef, Grzesiek et al. assumed a dynamic equilibrium only between a monomeric and a dimeric form. Under this assumption, they calculated the dissociation constant for the Nef$_{\Delta2–39,\Delta159–173}$ dimer to be 0.7 mM (Grzesiek et al., 1997), in the same range as the k_2 values extracted from our equilibrium data (corresponding dissociation constant 0.5 to 0.6 mM). Even though the affinity of Nef core molecules for each other appears to be modest in vitro, Nef core oligomerization might be promoted in vivo by subcellular colocalization at the cell membrane. However, there is as yet no data documenting the levels of expression of Nef in infected cells. Additionally, interactions between the unstructured N-termini and the core domains may reinforce the stability of the oligomers. The isolated N-termini seem not to form defined oligomers in vitro, as they appear monomeric and tend to aggregate when myristoylated (Geyer et al., 1999).

In vitro, the first 57 amino-terminal residues of HIV-1 Nef promote formation of large aggregates. It is intriguing that proteolytic cleavage of Nef by the viral protease leads to a fragment with drastically reduced tendency to aggregate. However, it cannot be excluded that in vivo post-translational modifications and membrane targeting strongly reduce this propensity to aggregate.

In SIV and HIV-2 Nef alleles, most amino acids that are involved in HIV-1 Nef core oligomerization are conserved or homologous. However, the substitution of F121 in SIV/HIV-2 by an isoleucine, valine, or methionine might decrease the hydrophobic contact surface significantly. Moreover, some residues of the HIV-1 homomer interface are nonconservatively replaced in HIV-2 and SIV Nef. Especially the substitutions Y115 $\rightarrow$ E, D and H116 $\rightarrow$ R present in HIV-2 and SIV Nef will lead to an unfavorable proximity and burial of charges at the interface and disrupt the hydrophobic core of the oligomer interface. In consequence, if HIV-2 and SIV Nef alleles form oligomers analogous to HIV-1 Nef, they might be either less stable or be stabilized differently, for example, via their N-termini. If the homomer formation is relevant for the action of HIV-1 Nef, it may be possible that discrepancies in the oligomeric state contribute in part to observed differences in the action of HIV-1 and SIV Nef proteins, i.e., down-regulation of MHC-I and CD4, and direct association with TCR zeta chain (Howe et al., 1998; Xu et al., 1999). This, however, awaits further experimental evidence.

Nef core oligomers: A role in vivo?

Several amino acids of the herein outlined dimer and trimer interface have been mutated and phenotypically characterized. Man-

ninen et al. (1998) reported that that the mutations L112R and F121R affected the binding of the Nef-associated kinases (NAK) to Nef. Liu et al. showed that each of the Nef point mutants D108A, D111G, L112D, F121G, P122R, and D123G was unable to interact with a human thioesterase and to down-regulate CD4. In addition, the single point mutant Nef D123G was also defective for MHC-I down-modulation (Liu et al., 2000). This is especially intriguing as (1) CD4 and MHC-I down-regulation appeared to date to be functionally and genetically distinct and (2) none of the mutations affects the putative CD4 binding site mapped by Grzesiek et al. (1996b). A unifying explanation for the numerous effects of these mutations may be that they destabilize the oligomeric state of Nef, which may be required for efficient interaction with this subset of its cellular targets. Liu et al. (2000) reported that the mutation of the residue D123 is sufficient to disrupt the dimeric association of CD8-Nef fusion proteins. In the Nef oligomers, but not in the Nef monomers, D123 is interacting with the conserved di-arginine motif $R^{105}R^{106}$ of another protomer. This di-arginine motif is required for CD4 down-regulation (Wiskerchen & Cheng-Mayer, 1996; Iafrate et al., 1997) and for the interaction of Nef with NAK (Sawai et al., 1996).

Although the biological significance of these self-association processes remains obscure, it is expected that such mechanisms could participate in various Nef–cellular target interactions. Like Nef itself, many of its possible targets are localized at the cell membrane (CD4, MHC-I, TCR zeta, Src kinases). Nearly all putative cellular partners of Nef are either implicated in signal transduction pathways or are part of the endocytic machinery (Cullen, 1998). Oligomerization is a biological regulatory mechanism employed by both soluble and membrane proteins (Klemm et al., 1998): signaling is frequently initiated by dimerization of transmembrane receptors. Interestingly, cellular targets of Nef, such as CD4 (Wu et al., 1997), MHC-I (Capps et al., 1993), the μ chain of the AP adapter complex (Owen & Evans, 1998), and the TCR zeta chain (Garcia et al., 1999) are dimeric when activated. As binding energies are additive, a dimeric or trimeric Nef may gain affinity for an oligomeric partner, leading to a more efficient interaction. Oligomerization of Nef may also provide a tool to link proteins that are associated with Nef (i.e., TCR and Src kinases), thus stimulating a functional interaction between Nef-bound molecules.

Molecular epidemiology studies are frequently funded on the analysis of specific amino acid substitutions in *nef* gene derived from individuals infected with HIV-1 virus with different stages of disease and, in particular, long-term survivors of HIV-1 infection. Our data offer the opportunity to focus these analysis on new biological functional sites involved in oligomerization of Nef. The molecular models for Nef core dimers and trimers proposed here should also provide targets for further mutational studies to elucidate the functional role of Nef homomers. If the oligomeric state of Nef influences its action, the interface between adjacent Nef molecules may serve as a novel target for the design of anti-viral agents.

Materials and methods

Protein preparation

The expression and purification of Nef full length and $\text{Nef}_{\Delta 1,57}$ have been described earlier (Franken et al., 1997). The *nef* gene fragment corresponding to Nef $\text{Nef}_{\Delta 1-56, \Delta 206}$ was isolated by the polymerase chain reaction (PCR) using two oligonucleotide prim-

ers and digested using BamHI-EcoRI. The resulting fragment was cloned into pGEX-2T expression vector (Pharmacia, Uppsala, Sweden). The protein was expressed as an N-term GST fusion protein in the *Escherichia coli* strain BL21(DE3). Recombinant $\text{Nef}_{\Delta 1-56, \Delta 206}$ was purified as previously described (Franken et al., 1997).

Dynamic light scattering

DLS experiments were performed at 20 °C with a Brookhaven Instrument, as previously described (Boyer et al., 1996). The wavelength of 514 nm was produced by an argon ion laser from Spectra Physics (Mountain View, California), running at a power of 200 mW. The scattered laser light was collected at an angle of 908 from the incident beam. Two programs provided by Brookhaven Instrument (Holtsville, New York) were used to determine the protein size: the method of cumulants (Koppel, 1972), which gives an apparent diameter and an index of polydispersity and NNLS (Non-Negatively-constrained Least Squares) analysis (Morrison et al., 1985), which gives an intensity weighted size distribution. Molecular weights were calculated from scattered light intensities, using a refractive index increment of 0.19 mL/g, a typical value for most proteins (Wen et al., 1996). Solutions of purified Nef proteins were prepared in 10 mM Tris-HCl buffer at pH 7.5, 100 mM NaCl, and 2 mM EGTA. For full length and $\text{Nef}_{\Delta 1,57}$ 5 mM DTT were added. Prior to DLS experiments, protein solutions were centrifuged at $45,000 \times g$ for 30 min at 4 °C and passed through a Millipore filters with a pore size of 0.1 μm to eliminate dust particles and large aggregates.

NMR spectroscopy

For NMR spectroscopy, $\text{Nef}_{\Delta 1-56, \Delta 206}$ was kept in 20 mM sodium phosphate buffer, 100 mM NaCl, pH 7.5, and 90% H_2O/10% D_2O. NMR experiments were carried out on a Bruker AMX 600 MHz instrument, equipped with a triple resonance probe, delivering field gradient along the z axis up to 50 G/cm. We used the LED pulse sequence (Wu et al., 1995) with a presaturation during relaxation and diffusion delays, and watergate excitation. The diffusion delay was 200 ms and gradient duration was chosen between 1.4 and 3 ms. Two-dimensional DOSY spectra have been collected at 22.8 °C. Thirty-six values of gradient intensity were used for each measure, ranging from 2–95% of the full gradient intensity. Data were processed and analyzed using the Gifa program (Pons et al., 1996) on SGI and HP workstations. All data were analyzed using the Maximum Entropy algorithms (Delsuc & Malliavin, 1998).

To obtain a relation between diffusion coefficient and SASA or molecular weight, the diffusion coefficients of a set of 15 proteins were correlated with their calculated solvent accessible surface area (SASA) or their molecular weight, by least-squares regression (correlation factor 0.982 and 0.990, respectively). The SASA for the models was calculated using a rolling sphere of a radius of 1.4 Å as a probe, using the program Areaimol (CCP4, 1994).

Analytical ultracentrifugation

Experiments were carried out at 20 °C with a Beckman Optima XL-A analytical ultracentrifuge equipped with a four-hole An-55 rotor and standard 1.2 cm hexa-sector cells. The samples of the $\text{Nef}_{\Delta 1-56, \Delta 206}$ core domain were prepared in 20 mM Tris-HCl buffer, pH 7.5, 100 mM NaCl. Protein concentration distributions were determined at 302 nm to keep the absorbance below 1.5 in the cell

at equilibrium. Samples were run at 15,000 rpm for six different concentrations (0.1, 0.23, 0.37, 0.45, 0.6, and 0.8 mM) and 12,000 rpm for two different concentrations (0.23 and 0.45 mM). Data were acquired over a 40 h period as averages of 10 measurements of absorbance data in the step scan mode, with a radial step size of 0.003 cm. Data sets were collected after reaching equilibrium, judged to be achieved by the absence of systematic deviations between the successive scans taken 2 h apart after the initial ∼20 h equilibration. Sedimentation equilibrium data and protein distribution were analyzed and evaluated using a nonlinear least-squares curve-fitting algorithm contained in the MicroCal Origin-based Optima XL-A software (Beckman, Fullerton, California). The data, absorbance vs. radial distance, were analyzed using the different fitting models for a single homogeneous species and a self-associating system (monomer-dimer-n-mer). Association constants were calculated by a simultaneous fit of eight datasets to a single set of constants. Criteria for a good fit included random distribution of residuals and minimized residuals. The associated RMS is defined as the square root of the variance of the fit and expressed in optical density units. A partial specific volume of 0.731 mL/g for Nef core domain was calculated from the amino acid composition (Laue et al., 1992). The solvent density was set to 1.0. The association constants were converted to units of M^{-1} using a Nef molar extinction coefficient equal to 5,811 at the selected wavelength.

Chemical cross-linking

Samples of Nef core domain ($Nef_{\Delta1-56,\Delta206}$) were reacted to completion (overnight) with 2% glutaraldehyde at room temperature, in 50 mM phosphate buffer, pH 8.0. Cross-linked samples were boiled for 5 min with SDS sample buffer (4% SDS, 3% β-mercaptoethanol, 0.01% bromophenol blue) and analyzed by SDS PAGE electrophoresis in 12% polyacrylamide, under standard denaturing conditions. The molecular weight markers were prepared under denaturing conditions as outlined by the manufacturers.

Structural analysis

Coordinate files were taken from the Protein Data Bank (PDB). Trimeric Nef core was obtained from the crystal structure of free $Nef_{\Delta1,57}$ (PDB access code 1avv) by generating crystallographic symmetry related molecules. Crystal structures of Nef in a complex with Src family SH3 domains (PDB access codes 1efn and 1avz) contain dimeric Nef core. Model structures of SIVmac239 and HIV-2rod Nef core domains were built on the basis of HIV-1 Nef crystal structures as described in Arold et al. (1998). As crystal structures of $Nef_{\Delta1,57}$ lack residues 56–70, 149–177, and 203–206, the NMR model of HIV-1 $Nef_{\Delta2-39,\Delta159-173}$ (PDB access code 2nef) was used as a template to build models for $Nef_{\Delta1,57}$, $Nef_{\Delta1-56,\Delta206}$ and $Nef_{\Delta1-56,\Delta149-177,\Delta206}$ for SASA calculation. Molecular surface analysis of the coordinate files was carried out using GRASP (Nicholls et al., 1991) and AESOP (M.E. Noble, unpubl. data). AESOP was also used for calculating and visualizing the "hydrophobic potential" of the molecules (defined as the energy $W(x,y,z)$ associated with placing a hydrophobic probe on x,y,z on the surface of the protein).

Acknowledgments

References

Aiken C, Konner J, Landau NR, Lenburg ME, Trono D. 1994. Nef induces CD4 endocytosis: Requirement for a critical dileucine motif in the membrane-proximal CD4 cytoplasmic domain. *Cell* 76:853–864.

Arold S, Franken P, Strub MP, Hoh F, Benichou S, Benarous R, Dumas C. 1997. The crystal structure of HIV-1 Nef protein bound to the Fyn kinase SH3 domain suggests a role for this complex in altered T cell receptor signaling. *Structure* 5:1361–1372.

Arold S, O'Brien R, Franken P, Hoh F, Strub M-P, Dumas C, Ladbury J. 1998. RT loop flexibility enhances the specificity of Src family SH3 domains for HIV-1 Nef. *Biochemistry* 37:14683–14691.

Barnham KJ, Monks SA, Hinds MG, Azad AA, Norton RS. 1997. Solution structure of a polypeptide from the N terminus of the HIV protein Nef. *Biochemistry* 36:5970–5980.

Baur AS, Sawai ET, Dazin P, Fantl WJ, Cheng-Mayer C, Peterlin BM. 1994. HIV-1 Nef leads to inhibition or activation of T cells depending on its intracellular localization. *Immunity* 1:373–384.

Benichou S, Bomsel M, Bodeus M, Durand H, Doute M, Letourneur F, Camonis J, Benarous R. 1994. Physical interaction of the HIV-1 Nef protein with beta-COP, a component of non-clathrin-coated vesicles essential for membrane traffic. *J Biol Chem* 269:30073–30076.

Boyer M, Roy MO, Jullien M. 1996. Dynamic light scattering study of precrystallizing ribonuclease solutions. *J Crystal Growth* 167:212–220.

Bresnahan PA, Yonemoto W, Ferrell S, Williams-Herman D, Geleziunas R, Greene WC. 1998. A dileucine motif in HIV-1 Nef acts as an internalization signal for CD4 downregulation and binds the AP-1 clathrin adaptor. *Curr Biol* 8:1235–1238.

Capps GG, Robinson BE, Lewis KD, Zuniga MC. 1993. In vivo dimeric association of class I MHC heavy chains. Possible relationship to class I MHC heavy chain-beta 2-microglobulin dissociation. *J Immunol* 151:159–169.

Carugo O, Argos P. 1997. Protein-protein crystal-packing contacts. *Protein Sci* 6:2261–2263.

CCP4 (Collaborative Computational Project Number 4). 1994. The CCP4 suite: Programs for protein crystallography. *Acta Crystallogr D50*:760–763.

Chen YL, Trono D, Camaur D. 1998. The proteolytic cleavage of human immunodeficiency virus type 1 Nef does not correlate with its ability to stimulate virion infectivity. *J Virol* 72:3178–3184.

Chothia C, Janin J. 1975. Principles of protein-protein recognition. *Nature* 256:705–708.

Chowers MY, Spina CA, Kwoh TJ, Fitch NJ, Richman DD, Guatelli JC. 1994. Optimal infectivity in vitro of human immunodeficiency virus type 1 requires an intact nef gene. *J Virol* 68:2906–2914.

Collette Y, Dutartre H, Benziane A, Ramos MF, Benarous R, Harris M, Olive D. 1996. Physical and functional interaction of Nef with Lck. HIV-1 Nef-induced T-cell signaling defects. *J Biol Chem* 271:6333–6341.

Conte LL, Chothia C, Janin J. 1999. The atomic structure of protein-protein recognition sites. *J Mol Biol* 285:2177–2198.

Craig HM, Pandori MW, Guatelli JC. 1998. Interaction of HIV-1 Nef with the cellular dileucine-based sorting pathway is required for CD4 down-regulation and optimal viral infectivity. *Proc Natl Acad Sci USA* 95:11229–11234.

Cullen BR. 1998. HIV-1 auxiliary proteins: Making connections in a dying cell. *Cell* 93:685–692.

Deacon NJ, Tsykin A, Solomon A, Smith K, Ludford-Menting M, Hooker DJ, McPhee DA, Greenway AL, Ellett A, Chatfield C, et al. 1995. Genomic structure of an attenuated quasi species of HIV-1 from a blood transfusion donor and recipients. *Science* 270:988–991.

Delsuc MA, Malliavin TE. 1998. Maximum entropy processing of DOSY NMR spectra. *Anal Chem* 70:2146–2148.

Du Z, Lang SM, Sasseville VG, Lackner AA, Ilyinskii PO, Daniel MD, Jung JU, Desrosiers RC. 1995. Identification of a nef allele that causes lymphocyte activation and acute disease in macaque monkeys. *Cell* 82:665–674.

Franken P, Arold S, Padilla A, Bodeus M, Hoh F, Strub MP, Boyer M, Jullien M, Benarous R, Dumas C. 1997. HIV-1 Nef protein: Purification, crystallizations, and preliminary X-ray diffraction studies. *Protein Sci* 6:2681–2683.

Freund J, Kellner R, Houthaeve T, Kalbitzer HR. 1994a. Stability and proteolytic domains of Nef protein from human immunodeficiency virus (HIV) type 1. *Eur J Biochem* 221:811–819.

Freund J, Kellner R, Konvalinka J, Wolber V, Krausslich HG, Kalbitzer HR. 1994b. A possible regulation of negative factor (Nef) activity of human

immunodeficiency virus type 1 by the viral protease. *Eur J Biochem* 223:589–593.

Fujii Y, Otake K, Fujita Y, Yamamoto N, Nagai Y, Tashiro M, Adachi A. 1996. Clustered localization of oligomeric Nef protein of human immunodeficiency virus type 1 on the cell surface. *FEBS Lett* 395:257–261.

Gaedigk-Nitschko K, Schon A, Wachinger G, Erfle V, Kohleisen B. 1995. Cleavage of recombinant and cell derived human immunodeficiency virus 1 (HIV-1) Nef protein by HIV-1 protease. *FEBS Lett* 357:275–278.

Garcia Bernal JM, Garcia de la Torre J. 1981. Transport properties of oligomeric subunit structures. *Biopolymers* 20:129–139.

Garcia JV, Miller AD. 1994. Retrovirus vector-mediated transfer of functional HIV-1 regulatory genes. *AIDS Res Hum Retroviruses* 10:47–52.

Garcia KC, Teyton L, Wilson IA. 1999. Structural basis of T cell recognition. *Annu Rev Immunol* 17:369–397.

Geyer M, Munte CE, Schorr J, Kellner R, Kalbitzer HR. 1999. Structure of the anchor-domain of myristoylated and non-myristoylated HIV-1 Nef protein. *J Mol Biol* 289:123–138.

Greenberg M, DeTulleo L, Rapoport I, Skowronski J, Kirchhausen T. 1998a. A dileucine motif in HIV-1 Nef is essential for sorting into clathrin-coated pits and for downregulation of CD4. *Curr Biol* 8:1239–1242.

Greenberg ME, Bronson S, Lock M, Neumann M, Pavlakis GN, Skowronski J. 1997. Co-localization of HIV-1 Nef with the AP-2 adaptor protein complex correlates with Nef-induced CD4 down-regulation. *EMBO J* 16:6964–6976.

Greenberg ME, Iafrate AJ, Skowronski J. 1998b. The SH3 domain-binding surface and an acidic motif in HIV-1 Nef regulate trafficking of class I MHC complexes. *EMBO J* 17:2777–2789.

Greenway A, Azad A, McPhee D. 1995. Human immunodeficiency virus type 1 Nef protein inhibits activation pathways in peripheral blood mononuclear cells and T-cell lines. *J Virol* 69:1842–1850.

Grzesiek S, Bax A, Clore GM, Gronenborn AM, Hu JS, Kaufman J, Palmer I, Stahl SJ, Wingfield PT. 1996a. The solution structure of HIV-1 Nef reveals an unexpected fold and permits delineation of the binding surface for the SH3 domain of Hck tyrosine protein kinase. *Nat Struct Biol* 3:340–345.

Grzesiek S, Bax A, Hu JS, Kaufman J, Palmer I, Stahl SJ, Tjandra N, Wingfield PT. 1997. Refined solution structure and backbone dynamics of HIV-1 Nef. *Protein Sci* 6:1248–1263.

Grzesiek S, Stahl SJ, Wingfield PT, Bax A. 1996b. The CD4 determinant for downregulation by HIV-1 Nef directly binds to Nef. Mapping of the Nef binding surface by NMR. *Biochemistry* 35:10256–10261.

Hanna Z, Kay DG, Rebai N, Guimond A, Jothy S, Jolicoeur P. 1998. Nef harbors a major determinant of pathogenicity for an AIDS-like disease induced by HIV-1 in transgenic mice. *Cell* 95:163–175.

Harris MP, Neil JC. 1994. Myristoylation-dependent binding of HIV-1 Nef to CD4. *J Mol Biol* 241:136–142.

Hensley P. 1996. Defining the structure and stability of macromolecular assemblies in solution: The re-emergence of analytical ultracentrifugation as a practical tool. *Structure* 4:367–373.

Howe AY, Jung JU, Desrosiers RC. 1998. Zeta chain of the T-cell receptor interacts with nef of simian immunodeficiency virus and human immunodeficiency virus type 2. *J Virol* 72:9827–9834.

Iafrate AJ, Bronson S, Skowronski J. 1997. Separable functions of Nef disrupt two aspects of T cell receptor machinery: CD4 expression and CD3 signaling. *EMBO J* 16:673–684.

Janin J, Chothia C. 1990. The structure of protein-protein recognition sites. *J Biol Chem* 265:16027–16030.

Janin J, Rodier F. 1995. Protein-protein interaction at crystal contacts. *Proteins* 23:580–587.

Johnson CS, Gabriel DA. 1981. NMR spectroscopy. In: Bell EJ, ed. *Spectroscopy in biochemistry*, Vol. 2. Boca Raton, Florida: CRC Press. p 178.

Johnson ML, Correia JJ, Yphantis DA, Halvorson HR. 1981. Analysis of data from the analytical ultracentrifuge by nonlinear least-squares techniques. *Biophys J* 36:575–588.

Jones S, Thornton JM. 1997. Analysis of protein-protein interaction sites using surface patches. *J Mol Biol* 272:121–132.

Kienzle N, Freund J, Kalbitzer HR, Mueller-Lantzsch N. 1993. Oligomerization of the Nef protein from human immunodeficiency virus (HIV) type 1. *Eur J Biochem* 214:451–457.

Kirchhoff F, Greenough TC, Brettler DB, Sullivan JL, Desrosiers RC. 1995. Brief report: Absence of intact nef sequences in a long-term survivor with nonprogressive HIV-1 infection. *N Engl J Med* 332:228–232.

Klemm JD, Schreiber SL, Crabtree GR. 1998. Dimerization as a regulatory mechanism in signal transduction. *Annu Rev Immunol* 16:569–592.

Koppel DE. 1972. Analysis of macromolecular polydispersity in intensity correlation spectroscopy: The methods of cumulants. *J Chem Phys* 57:4814–4820.

Krishnan VV, Cosman M. 1998. An empirical relationship between rotational correlation time and solvent accessible surface area. *J Biomol NMR* 12:177–182.

Laue TM, Shah BD, Ridgeway TM, Pelletier SL. 1992. Computer-aided interpretation of omalytical sedimentation data for protins. In: Harding SR, Rowe AJ, Horton JC, eds. *Analytical ultracentrifugation in biochemistry and polymer science*. Cambridge, UK: The Royal Society of Chemistry. pp 90–125.

Lee CH, Leung B, Lemmon MA, Zheng J, Cowburn D, Kuriyan J, Saksela K. 1995. A single amino acid in the SH3 domain of Hck determines its high affinity and specificity in binding to HIV-1 Nef protein. *EMBO J* 14:5006–5015.

Lee CH, Saksela K, Mirza UA, Chait BT, Kuriyan J. 1996. Crystal structure of the conserved core of HIV-1 Nef complexed with a Src family SH3 domain. *Cell* 85:931–942.

Le Gall S, Erdtmann L, Benichou S, Berlioz-Torrent C, Liu L, Benarous R, Heard JM, Schwartz O. 1998. Nef interacts with the mu subunit of clathrin adaptor complexes and reveals a cryptic sorting signal in MHC I molecules. *Immunity* 8:483–495.

Liu LX, Heveker N, Fackler OT, Arold S, Le Gall S, Janvier K, Peterlin BM, Dumas C, Schwartz O, Benichou S, Benarous R. 2000. Mutation of a conserved residue (D123) required for oligomerization of human immunodeficiency virus type 1 nef protein abolishes interaction with human thioesterase and results in impairment of nef biological functions. *J Virol* 74:5310–5319.

Liu LX, Margottin F, Le Gall S, Schwartz O, Selig L, Benarous R, Benichou S. 1997. Binding of HIV-1 Nef to a novel thioesterase enzyme correlates with Nef-mediated CD4 down-regulation. *J Biol Chem* 272:13779–13785.

Manninen A, Hiipakka M, Vihinen M, Lu W, Mayer BJ, Saksela K. 1998. SH3-Domain binding function of HIV-1 Nef is required for association with a PAK-related kinase. *Virology* 250:273–282.

Mariani R, Kirchhoff F, Greenough TC, Sullivan JL, Desrosiers RC, Skowronski J. 1996. High frequency of defective nef alleles in a long-term survivor with nonprogressive human immunodeficiency virus type 1 infection. *J Virol* 70:7752–7764.

Miller MD, Feinberg MB, Greene WC. 1994. The HIV-1 nef gene acts as a positive viral infectivity factor. *Trends Microbiol* 2:294–298.

Miller MD, Warmerdam MT, Ferrell SS, Benitez R, Greene WC. 1997. Intravirion generation of the C-terminal core domain of HIV-1 Nef by the HIV-1 protease is insufficient to enhance viral infectivity. *Virology* 234:215–225.

Morrison ID, Grabowski EF, Herb CA. 1985. Improved techniques for particle size determination by quasi elastic light scattering. *Langmuir* 1:496–501.

Nicholls A, Sharp KA, Honig B. 1991. Protein folding and association: Insights from the interfacial and thermodynamic properties of hydrocarbons. *Proteins* 11:281–296.

Owen DJ, Evans PR. 1998. A structural explanation for the recognition of tyrosine-based endocytotic signals. *Science* 282:1327–1332.

Pandori MW, Fitch NJ, Craig HM, Richman DD, Spina CA, Guatelli JC. 1996. Producer-cell modification of human immunodeficiency virus type 1: Nef is a virion protein. *J Virol* 70:4283–4290.

Piguet V, Chen YL, Mangasarian A, Foti M, Carpentier JL, Trono D. 1998. Mechanism of Nef-induced CD4 endocytosis: Nef connects CD4 with the mu chain of adaptor complexes. *EMBO J* 17:2472–2481.

Piguet V, Gu F, Foti M, Demaurex N, Gruenberg J, Carpentier JL, Trono D. 1999. Nef-induced CD4 degradation: A diacidic-based motif in Nef functions as a lysosomal targeting signal through the binding of beta-COP in endosomes. *Cell* 97:63–73.

Pons JL, Malliavin T, Delsuc MA. 1996. Gifa V4: A complete package for NMR data-set processing. *J Biomol NMR* 8:445–452.

Rossi F, Gallina A, Milanesi G. 1996. Nef-CD4 physical interaction sensed with the yeast two-hybrid system. *Virology* 217:397–403.

Saksela K. 1997. HIV-1 Nef and host cell protein kinases. *Front Biosci* 2:606–618.

Saksela K, Cheng G, Baltimore D. 1995. Proline-rich (PxxP) motifs in HIV-1 Nef bind to SH3 domains of a subset of Src kinases and are required for the enhanced growth of Nef+ viruses but not for down-regulation of CD4. *EMBO J* 14:484–491.

Sawai ET, Khan IH, Montbriand PM, Peterlin BM, Cheng-Mayer C, Luciw PA. 1996. Activation of PAK by HIV and SIV Nef: Importance for AIDS in rhesus macaques. *Curr Biol* 6:1519–1527.

Schorr J, Kellner R, Fackler O, Freund J, Konvalinka J, Kienzle N, Krausslich HG, Mueller-Lantzsch N, Kalbitzer HR. 1996. Specific cleavage sites of Nef proteins from human immunodeficiency virus types 1 and 2 for the viral proteases. *J Virol* 70:9051–9054.

Schwartz O, Marechal V, Danos O, Heard JM. 1995. Human immunodeficiency virus type 1 Nef increases the efficiency of reverse transcription in the infected cell. *J Virol* 69:4053–4059.

Schwartz O, Marechal V, Le Gall S, Lemonnier F, Heard JM. 1996. Endocytosis of major histocompatibility complex class I molecules is induced by the HIV-1 Nef protein. *Nat Med* 2:338–342.

Welker R, Kottler H, Kalbitzer HR, Krausslich HG. 1996. Human immunodeficiency virus type 1 Nef protein is incorporated into virus particles and specifically cleaved by the viral proteinase. *Virology 219*:228–236.

Wen J, Arakawa T, Philo JS. 1996. Size-exclusion chromatography with on-line light-scattering, absorbance, and refractive index detectors for studying proteins and their interactions. *Anal Biochem 240*:155–166.

Wiskerchen M, Cheng-Mayer C. 1996. HIV-1 Nef association with cellular serine kinase correlates with enhanced virion infectivity and efficient proviral DNA synthesis. *Virology 224*:292–301.

Wray V, Mertins D, Kiess M, Henklein P, Trowitzsch-Kienast W, Schubert U. 1998. Solution structure of the cytoplasmic domain of the human CD4 glycoprotein by CD and 1H NMR spectroscopy: Implications for biological functions. *Biochemistry 37*:8527–8538.

Wu DH, Chen AD, Johnson CS. 1995. An improved diffusion-ordered spectroscopy experiment incorporating bipolar-gradient pulses. *J Magn Reson Ser A 115*:260–264.

Wu H, Kwong PD, Hendrickson WA. 1997. Dimeric association and segmental variability in the structure of human CD4. *Nature 387*:527–530.

Xu XN, Laffert B, Screaton GR, Kraft M, Wolf D, Kolanus W, Mongkolsapay J, McMichael AJ, Baur AS. 1999. Induction of Fas ligand expression by HIV involves the interaction of Nef with the T cell receptor zeta chain. *J Exp Med 189*:1489–1496.